Journal of Nuclear Materials 467 (2015) 229–239

Contents lists available at ScienceDirect

Journal of Nuclear Materials

journal homepage: www.elsevier.com/locate/jnucmat

Atomic interaction of the MEAM type for the study of intermetallics in the Al–U alloy

M.I. Pascuet [a], J.R. Fernández [a, b, c, *]

[a] CONICET, Avda. Rivadavia 1917, 1033 Buenos Aires, Argentina
[b] CAC-CNEA, Avda. Gral Paz 1499, 1650 Buenos Aires, Argentina
[c] UNSAM, Avda. Gral Paz 1499, 1650 Buenos Aires, Argentina

HIGHLIGHTS

- Potential parameters for Al and Al–U systems are obtained.
- Intermetallics are characterized by calculating elastic and thermal properties.
- Point defect diffusivities are calculated for the three intermetallics.
- Growth of the Al_3U intermetallic is shown to occur in the Al/U interface as in the real alloy.

ARTICLE INFO

Article history:
Received 8 May 2015
Received in revised form
5 August 2015
Accepted 16 September 2015
Available online 18 September 2015

Keywords:
Aluminum
Uranium
MEAM interatomic potential
Computer simulation

ABSTRACT

Interaction for both pure Al and Al–U alloys of the MEAM type are developed. The obtained Al interatomic potential assures its compatibility with the details of the framework presently adopted. The Al–U interaction fits various properties of the Al_2U, Al_3U and Al_4U intermetallics. The potential verifies the stability of the intermetallic structures in a temperature range compatible with that observed in the phase diagram, and also takes into account the greater stability of these structures relative to others that are competitive in energy. The intermetallics are characterized by calculating elastic and thermal properties and point defect parameters. Molecular dynamics simulations show a growth of the Al_3U intermetallic in the Al/U interface in agreement with experimental evidence.

1. Introduction

In the last decades, the metallic U–Mo alloy has been considered as a prototype of nuclear fuel of high U density [1–3]. In practice, the U–Mo alloy is dispersed in an Al matrix, which acts as a mechanical support and allows fast transmission of heat generated by fission. During the irradiation, the fuel particles react with the surrounding Al matrix and post-irradiation experiments have shown a significant interaction layer producing a considerable swelling and unacceptable porosity [4]. Many works have been dedicated to identify phase products in the interaction layer and to study their formation dynamics [5–8], while others focus on how to avoid or lessen their occurrence, mainly by adding elements like Si to the Al matrix and transition elements to the fuel alloy [9,10]. The investigations carried out to reach a solution of the technological problems are not usually based on scientific grounds and relay on comparisons with other similar systems or just trial and error.

Diffusion experiments between Al and U have been carried out since the end of 1940's by a number of authors to measure the growth rate of the interaction band at different temperatures and pressures. Many of the works report that the diffusion zone is mainly formed by the Al_3U phase, which grows irregularly into U, and that Al_4U is porous and fragile while Al_2U and Al_3U form adherent layers. The applied pressure increases and the metal oxides inhibit the growth of the diffusion zone. Bareis [11] is one of the first works in reporting that clean surfaces of Al and U reacted under contact at moderate temperatures to form Al_3U. He found an increase of the interaction layer with the applied pressure and concluded that the formation of Al_3U is due to U diffusion through the Al_3U layer. Murray [12] prepared diffusion couples of Al/U by

* Corresponding author. Gerencia de Materiales, CAC, CNEA, Avda. Gral Paz 1499, 1650 Buenos Aires, Argentina.
E-mail address: julrfern@cnea.gov.ar (J.R. Fernández).

http://dx.doi.org/10.1016/j.jnucmat.2015.09.030
0022-3115/

dipping U samples in molten Al to get rid of oxide skins and to insure a good metallic contact between the two metals. She claimed that Al is the diffusing species and did not find any evidence of U diffusing into Al. Also, she observed formation of Al_3U in U cracks, concluding that diffusion in surface should be faster than in the bulk. Storchheim and Zambrow [13] also concluded from marker motion studies that Al diffuses faster into U than vice versa. They confirmed that the applied pressure helps to increase the rate of growth of Al_3U into Al. Le Claire and Bear [14] found that Al_3U is the main phase present in the diffusion zone, Al_2U is found to form a very thin layer between Al_3U and U and a gray powder formed under certain conditions between Al_3U and Al is identified as Al_4U. They observed that the diffusion band penetrated around 70% into Al and 30% into U with respect to the initial contact plane. Similar percentages (60% for Al and 40% for U) are observed by Deluca and Sumsion [15]. Castleman [16] established correlations between annealing time, annealing temperature, applied pressure and the nature and distribution of voids observed in Al_3U. He found that the rate of growth of Al_2U and Al_4U is much slower than that of Al_3U. Subramanyam et al. [5] studied the irregular growth of the diffusion band into U and proposed that interfacial breakdown is not a result of preferred growth direction, but rather due to both limited nucleation rate and high growth rate of the Al_3U phase.

Predicting the effects that degrade the material requires the knowledge of phenomena operating at atomic level, which is difficult to access by experiments. Atomistic simulation methods are important as a tool in supporting experiments, since they are able to separate the effects of various components of the evaluation of the microstructure and thus reveal fundamental physical mechanism of degradation. In this paper, Modified Embedded Atom Method (MEAM) [17,18] interatomic potentials are fitted for Al and Al–U binary system. The pure Al interatomic potential fitted in this work adapts better to the context of the present study than previous others found in the literature [19–21]. This potential, together with a recently developed MEAM potential for pure U [22], are used to find an appropriate interaction for the Al–U alloy. All reported simulations are performed by means of the LAMMPS code [23].

In Section 2 the main aspects of the MEAM formalism are briefly recalled. Then, a description of the fitting procedure to determine the MEAM parameters is given, and their optimal values for all the needed interactions are reported. Many different static and dynamic properties of the perfect lattice and microstructural defects for pure Al are given in Section 3 and for Al–U alloys in Section 4. Only the effect of single point defects have been studied, as the main purpose of the present work is to assess the potential performance in simple diffusion situations in which irradiation is absent. Results are compared with first principles, other classical potentials and experimental values from the literature, when available. Finally, in Section 5 all results are summarized.

2. Calculation method

2.1. MEAM formalism

A full description of the original MEAM formalism has been published elsewhere [24]. In this section, only the main aspects of the model are briefly described. In the MEAM, the total energy of a multicomponent system is approximated as:

$$E = \sum_i F_i(\overline{\rho}_i) + \frac{1}{2}\sum_{j\neq i}\phi_{ij}(R_{ij}), \tag{1}$$

F_i is the embedding function, $\overline{\rho}_i$ is the background electron density at site i, and ϕ_{ij} (R_{ij}) is the pair interaction between atoms i and j separated by a distance R_{ij}. The embedding function is given as:

$$F(\overline{\rho}) = AE_c\frac{\overline{\rho}}{\overline{\rho}^0}\ln\left[\frac{\overline{\rho}}{\overline{\rho}^0}\right], \tag{2}$$

where A is an adjustable parameter, E_c is the cohesion energy, and $\overline{\rho}^0$ is the background electron density for a reference structure. Generally, the low temperature experimental structure is taken as reference structure. The background electron density $\overline{\rho}_i$ is composed of a spherically symmetric partial electron density $\rho_i^{(0)}$ and angular contributions $\rho_i^{(1)}$, $\rho_i^{(2)}$ and $\rho_i^{(3)}$, representing the contributions of s, p, d and f atomic electron densities [24]. The partial electron densities are combined into:

$$\Gamma_i = \sum_{h=1}^{3} t^{(h)}\left[\rho_i^{(h)}\Big/\rho_i^{(0)}\right]^2. \tag{3}$$

where $t^{(h)}$ are adjustable parameters. The total electron density at site i is evaluated as:

$$\overline{\rho}_i = \rho_i^{(0)}G(\Gamma_i) \tag{4}$$

where $G(\Gamma) = \sqrt{1+\Gamma}$ for Al and $G(\Gamma) = 2/(1+e^{-\Gamma})$ for U. To calculate the pair term of Eq. (1) it is necessary to give a functional form to $\phi(R)$. However, there is no specific form in the MEAM formalism. Its value is computed from the difference of the total energy and the embedding function as a function of distance R in the reference structure. The total energy per atom is obtained from the universal state equation of Rose et al. [25] as a function of R:

$$E^a(R) = -E_c\left(1 + a^* + da^{*3}\right)e^{-a^*} \tag{5}$$

where d is an adjustable parameter, $a^* = \alpha(R/r_e - 1)$, r_e is the first neighbor distance, $\alpha = (9B\Omega E_c)^{1/2}$, B is the bulk modulus and Ω is the equilibrium atomic volume. It should be noted that the parameter d can take two different values $d1$ and $d2$, accordingly if a^* is positive (expansion) or negative (contraction). The pair potential $\phi(R)$ is extracted by inverting the next expression, considering up to second neighbor interactions [18]:

$$E^a(R) = F\left[\overline{\rho}^0(R)\right] + (Z_1/2)\phi(R) + (Z_2S/2)\phi(aR), \tag{6}$$

where Z_i is the number of neighbors in the i-shell, a is the ratio between the first and second neighbor distance and S is the screening factor. Lee and Baskes [18] have shown the details of extracting $\phi(R)$ from the Eq. (6). The screening factor S represents the influence of the neighbor atoms k in the interaction between i and j. For each neighbor atom k, it is possible to calculate a C factor:

$$x^2 + \frac{1}{C}y^2 = \frac{R_{ij}^2}{4} \tag{7}$$

where x, y are the coordinates of k with respect to the ellipse defined by the positions i, j, k. The screening of the k atom varies gradually in the range $C_{min} < C < C_{max}$. If $C < C_{min}$ the screening is total ($S = 0$) and there is not direct interaction between i y j, while if $C > C_{max}$ the interaction is independent of k ($S = 1$) [18].

2.2. Determination of MEAM parameters

The parameters of the model are determined by minimizing the objective function:

$$Q = \sum_i w_i \frac{\left(q_i^{ref} - q_i^{calc}\right)^2}{\left(q_i^{ref}\right)^2} \quad (8)$$

where q_i^{ref} are reference values, q_i^{calc} are the calculated values by the MEAM interatomic potential and w_i are the corresponding weights. First, the fifteen parameters of pure Al are determined; then, the eleven corresponding to the Al–U alloy. The minimization is carried out using the downhill simplex method [26] which is very robust and do not require any derivatives of Q.

2.3. MEAM potential for pure Al

The potential parameters for Al are fit to literature values of several properties of the ground state fcc structure and a few other metastable states, point defect properties, and the fcc elastic constants. Vacancy and interstitial migration barriers are roughly estimated as the difference between the system with the Al jumping atom constrained to be in the middle of its migration path and the same system with the defect in equilibrium in each case. Full relaxation of all structures at a temperature $T = 0$ K is allowed at each optimization step. Table 1 reports the best parameter set, while Tables 2–4 show the fitted properties. The corresponding weights w_i for each target property are also reported. Energy hierarchy between different phases is given the highest weights, defect properties are assigned intermediate weights and the lowest values are placed on the elastic properties. The overall fitting achieved is quite good except for a few quantities (elastic constant C_{44}, the octahedral self-interstitial and the new orthorhombic metastable phase).

2.4. MEAM potential for Al–U

The MEAM potential parameters for Al–U are fitted to reproduce the lattice parameters and formation energies of the three intermetallics and their relative stability with respect to several other structures (cubic $L1_2$ and $D0_3$, Laves phases C14, C15 and C36 and cubic B1 and B2). Thermal stability of intermetallics proved to be a very difficult property to satisfy, particularly for Al_4U. A very simple three-step process is implemented to force this property into the parameter fitting. First, a minimization of atomic coordinates and lattice parameters at 0 K of a small block is made. Then, a very short molecular dynamics (MD) simulation at *NVE* and 1000 K is performed with the purpose of shaking atoms out of their equilibrium positions. Finally, the atomic coordinates are relaxed again and the structure energy is compared with that of the first minimization. If the structure is stable under the current potential parameters, atoms will return to the initial positions and energies will be the same up to numerical tolerance (10^{-7} eV/at). This test turned out to be fast and good enough to ensure a local stability for the three intermetallic structures. Particular attention is also paid to constitutional point defects in Al_4U, which are forced to give positive energy differences with respect to the perfect lattice (see Section 4.4.1. ahead for a description of these defects). Vacancy migration energy of Al in Al_3U is imposed to render a value of around 0.8 eV [15]. To fit it, the migration energy is estimated from five different positions of a constrained Al atom along its migration path between two neighbor Al vacancies. As in the case of the pure Al potential, full relaxation of each structure is performed. All these calculations are repeated at each optimization step. In decreasing order of weight values, the higher importance are given to intermetallic thermal stability, their formation energies, phase stability regarding other metastable phases, constitutional point defects in Al_4U and Al migration in Al_3U, and, finally, the intermetallic lattice parameters.

The best set of potential parameters is reported in Table 5. Table 6 reports the calculated lattice parameters and formation energies for each intermetallic phase. Fig. 1 shows the relative intermetallics stabilities regarding other considered metastable

Table 1
Optimized potential parameters for Al. The reference structure is fcc.

α	$\beta^{(0)}$	$\beta^{(1)}$	$\beta^{(2)}$	$\beta^{(3)}$
4.68604	1.56205	5.39270	5.29601	−1.00047
a (Å)	E_c (eV)	A	t_1	t_2
4.05	3.36	1.06859	−1.54917	−1.28508
t_3	d_1	d_2	C_{min}	C_{max}
10.01041	0.39558	0.09806	1.00769	2.31407

Table 2
Calculated (MEAM), experimental (Exp.) and first principles (FP) lattice parameters and energies of different phases in Al. Target properties are in bold.

Structure	Property	MEAM	Exp./FP	w
A1, fcc	a (Å)	4.05	**4.050**[a]	500
			4.020[b]	
			4.036[c]	
	E_c (eV/at)	3.36	**3.360**[d]	50000
			4.074[b]	
A2, bcc	a (Å)	3.271	3.216[b]	
			3.240[c]	
	$\Delta E_{bcc-fcc}$ (eV/at)	0.159	**0.120**[d]	50000
			0.113[b]	
			0.087[c]	
A3, hcp	a (Å)	2.842	2.853[c]	
	c (Å)	4.734	4.681[c]	
	$\Delta E_{hcp-fcc}$ (eV/at)	0.040	**0.040**[d]	50000
			0.030[b]	
			0.033[c]	

[a] Ref. [27].
[b] Ref. [28].
[c] Ref. [29].
[d] Ref. [30].

Table 3
Calculated (MEAM), experimental (Exp.) and first principles (FP) formation volumes V^f, formation energies E^f, migration energies E^m, for vacancy and interstitials in Al. Target properties are in bold.

	MEAM	Exp./FP	w
V_V^f (Ω_{at})	0.716	**0.62**[a]	1
		0.7[b]	
E_V^f (eV)	0.670	**0.67 ± 0.03**[a]	500
		0.5–0.55[b]	
E_V^m (eV)	0.610	**0.61 ± 0.03**[a]	500
$V^f_{<100>}$ (Ω_{at})	3.144	**2.9**[a]	1
$E^f_{<100>}$ (eV)	2.992	**3.0**[a]	500
		2.7–2.43[b]	
$E^m_{<100>}$ (eV)	0.115	**0.115**[a]	500
ΔE^f_{Oct} (eV)	0.228	**>0.2**	50000
		0.1[b]	
ΔE^f_{Tet} (eV)	0.823	0.5[b]	

[a] Ref. [31].
[b] Ref. [21].

Table 4
Calculated (MEAM) and experimental (Exp.) elastic constant (GPa) in Al. Target values are in bold.

	MEAM	Exp. [32]	w
C_{11}	113.5	**11.43**	1
C_{12}	61.6	**61.92**	1
C_{44}	45.4	**31.62**	1

Table 5
Optimized potential parameters for Al–U. The reference structure is $L1_2$.

α	E_c (eV)	r_e (Å)	$\bar{\rho}^0_{U/Al}$	C_{min} (112)	C_{min} (121)
5.5364807	4.0435039	3.0432685	2.2488211	1.2094229	0.2558103
C_{min} (122)	C_{min} (221)	C_{max} (112)	C_{max} (121)	C_{max} (122)	C_{max} (221)
0.2019148	0.4418066	1.4792962	2.0880558	1.9424523	1.0510265

phases. The largest fitting errors with respect to the experimental values are found for Al_4U (around 3% for the lattice parameters and half the value for the formation energy).

3. Results for pure Al

3.1. Linear thermal expansion and melting temperature

To obtain the linear thermal expansion of pure Al, a temperature ramp from 250 K up to 1800 K is made for a block of 5 × 5 × 5 cubic unit cells ($N = 500$ atoms) for a relatively long simulation ($t = 10^4$ ps) at $P = 0$. The discontinuity in the atomic volume Ω vs temperature T at approximately 1200 K shown by Fig. 2 marks the end of the crystal order. Some overheating of the solid is to be expected, as no preferential nucleation site is provided. Once the solid is destabilized, the temperature drops to around the melting temperature and liquid becomes the new equilibrium state [39].

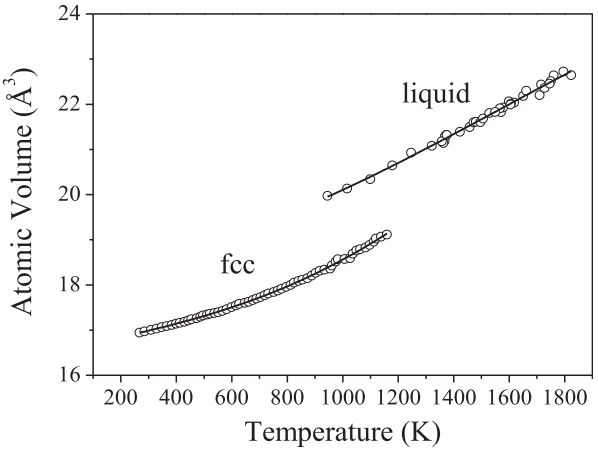

Fig. 2. Atomic volume as a function of temperature from a heating molecular dynamic simulation in Al.

By fitting a polynomial to each phase, the linear expansion coefficient can be obtained as $\alpha = 1/3\Omega \times \partial\Omega/\partial T$. Table 7 shows that the obtained values are larger than the available experimental data.

The coexistence phase method developed by Morris et al. [42] is applied to determine the melting temperature for the obtained potential. For this purpose, a large block of 4000 atoms is used. To obtain this large block, two sub-blocks (one in the fcc phase and the other in the liquid state) are built by juxtaposing four times the same cell of the previous temperature ramp simulation, before and after the melting has taken place. Then, the two sub-blocks are brought into contact arbitrarily in the [100] direction by appropriately rescaling the other two perpendicular edges. A short thermalization at constant *NPT* is performed at an initial estimation of T_m and $P = 0$ to remove as much stress as possible. Finally, the two-phase system is simulated at constant *NVE* for a relatively long time (10^3 ps) at several slightly different volumes. If both phases still exist at the end of the run, the resultant values of T and P will correspond to that of the equilibrium phase transformation. Extrapolation to $P = 0$ gives the melting temperature T_m. The Claussius–Clapeyron equation $dP/dT = L/T_m\Delta\Omega$ is used, to obtain the latent heat L by previously calculating $\Delta\Omega$ from Fig. 2 at the obtained T_m. Table 8 resumes all characterizing quantities for the melting of Al with the fitted potential.

3.2. Stacking faults

A stacking fault is an incorrect stacking in the sequence of (111)

Table 6
Calculated (MEAM), other interaction scheme (EAM), experimental (Exp.) and first principles (FP) lattice parameters and formation energies of the intermetallic phases in Al–U. Target properties are in bold.

Structure	Property	MEAM	EAM [33]	FP	Exp. [34]	w
Al_2U	a (Å)	7.672	7.585	7.674[a] 7.635[b] 7.629[c]	**7.760**	1000
	ΔE (eV/at)	−0.319	−0115	−0.127[b] −0.147[c]	**−0.319**	500000
Al_3U	a (Å)	4.271	4.166	4.266[d] 4.287[a] 4.238[b] 4.237[c]	**4.265**	1000
	ΔE (eV/at)	−0.263	−0.104	−0.096[b] −0.155[c]	**−0.281**	500000
Al_4U	a (Å)	4.501	4.128	4.356[b] 4.352[c]	**4.401**	1000
	b (Å)	6.109	6.470	6.197[b] 6.183[c]	**6.255**	1000
	c (Å)	13.775	13.691	13.671[b] 13.699[c]	**13.728**	1000
	ΔE (eV/at)	−0.137	−0.038	−0.039[b] −0.185[c]	**−0.258**	500000

[a] Ref. [35].
[b] Ref. [36].
[c] Ref. [37].
[d] Ref. [38].

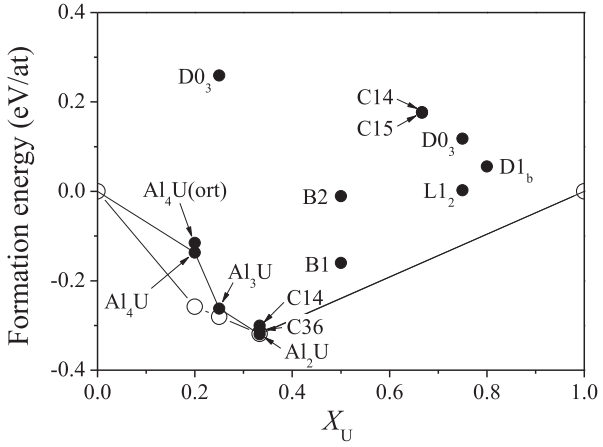

Fig. 1. Relative stability of the Al–U intermetallics. Full (open) circles correspond to calculated (experimental [34]) values. Structures are indicated by their strukturbericht symbol.

Table 7
Calculated (MEAM) and experimental (Exp.) linear thermal expansion for Al ($\times 10^{-5}$ 1/K) in solid (α_{fcc}) and liquid (α_{liq}) phases.

	MEAM	Exp.
α_{fcc} at 300 K	4.08	2.36[a]
α_{liq} at T_m	5.01	3.27[b]
		3.4–3.97[b]

[a] Ref. [40].
[b] Ref. [41].

Table 8
Calculated (MEAM) and experimental (Exp.) melting temperature, latent heat and volume change for Al.

	MEAM	Exp.
$dP/dT\|_{Tm}$ (MPa/K)	14	14.4[a]
		16.9[b]
T_m (K)	951	933.61[b]
$\Delta\Omega$ (cm^3/mol)	0.855 8.3%	0.729[c]
		6.4%[d]
L (J/mol)	11400	10580 ± 150[b]

[a] Ref. [43].
[b] Ref. [44].
[c] Ref. [45].
[d] Ref. [46].

compact planes in the fcc lattice. The stacking sequence in the perfect lattice is …ABCABCABC…, where A, B and C represent the usual different equilibrium positions in a compact plane of spheres. There are three different structure types for this defect. The *twin* fault, related to twin boundaries, with a sequence …ABCABC-BACBA… The *intrinsic* fault, formed when a plane of the sequence is missing, i.e., …ABCABC|BCABC…. And, finally, the *extrinsic* fault, when an extra compact (111) plane is inserted in the perfect sequence, …ABCABACABC… The defect energy is calculated as $\gamma_{SF} = \Sigma_i(E_i - E_c)/A$, where E_i is the energy of atom i evaluated through Eq. (1), A is the defect area and the sum extends over all atoms in the system containing the fault. Table 9 lists the calculated values for the different stacking faults. Their comparison with available experimental and first principles values [47] show a good correspondence.

3.3. Diffusion by vacancy mechanism

MD simulations for a system with one vacancy at different temperatures have been performed to calculate the diffusivity by vacancy mechanism in fcc Al. The mean square displacement $<r^2>$ of all atoms is recorded at regular times during the simulation and the diffusivity calculated through $D^* = \lim_{t\to\infty} <r^2>/6t$. Its behavior with T follows an Arrhenius form $D^* = D_0 \exp(-E^m/k_BT)$, from which a vacancy migration energy of $E^m = 0.66$ eV is obtained (Fig. 3). This result compares very well with that of Table 3 calculated statically.

4. Results for Al–U alloy

4.1. Elastic properties of intermetallics

Table 10 reports elastic constants and bulk modulus produced with the present MEAM potential for the three intermetallics. Bulk moduli calculations are obtained from simulations at different volumes rather than elastic constants averaging. Present calculations show systematically higher values than those available from first principles and experiment.

Table 9
Calculated (MEAM), first principles (FP) and experimental (Exp.) stacking fault energies (mJ/m^2) for pure Al.

	MEAM	FP [47]	Exp. [47]
Twin	93	5–130	75
Intrinsic	187	124–280	166
Extrinsic	187	108–260	

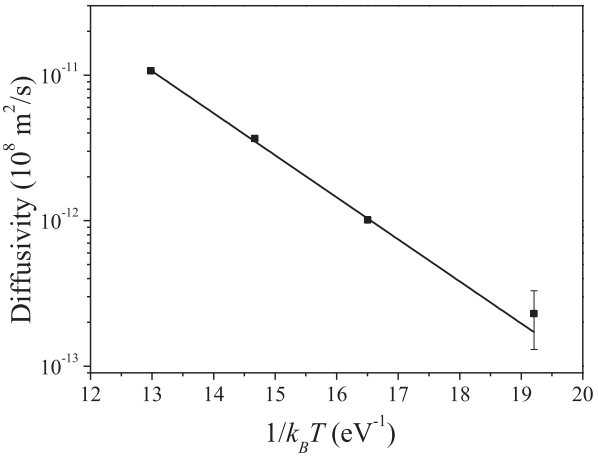

Fig. 3. Vacancy diffusivity as a function of temperature in fcc Al.

4.2. Temperature stability and thermal expansion of the Al–U intermetallics

Temperature ramps, as performed for pure Al, are made for each of the three Al–U intermetallics. Chosen block sizes are the same as previously described in Section 2.4. Simulations are run for 10^4 ps or more, continuously increasing the temperature from 100 K to 3000 K at $P = 0$. The atomic volume as a function of temperature in each case is given in Fig. 4. As in the case of pure Al, all simulations present an overheating of the solid phase and a sudden temperature drop at the start of the liquid phase [39]. Simulations show that

Table 10
Calculated (MEAM and FP) and experimental (Exp.) elastic constant and bulk modulus (GPa) in Al–U intermetallics.

	Property	MEAM	FP	Exp.
Al_2U	C_{11}	345	230[a]	
	C_{12}	103	38[a]	
	C_{44}	72	77[a]	
	B	183	111[b]	74[g]
			102[a]	83 ± 9[h]
			93[c]	
Al_3U	C_{11}	169	158[a]	
	C_{12}	96	50[a]	
	C_{44}	51	81[a]	
	B	120	98.07[d]	68 ± 7[h]
			94[b]	
			81.57[e]	
			86[a]	
			90[c]	
Al_4U	C_{11}	164		
	C_{22}	183		
	C_{33}	171		
	C_{12}	102		
	C_{13}	74		
	C_{23}	80		
	C_{44}	30		
	C_{55}	26		
	C_{66}	54		
	B	113	94[b]	73 ± 5[h]
			84[f]	
			88[c]	

[a] Ref. [35].
[b] Ref. [36].
[c] Ref. [37].
[d] Ref. [48].
[e] Ref. [38].
[f] Ref. [49].
[g] Ref. [50].
[h] Ref. [51].

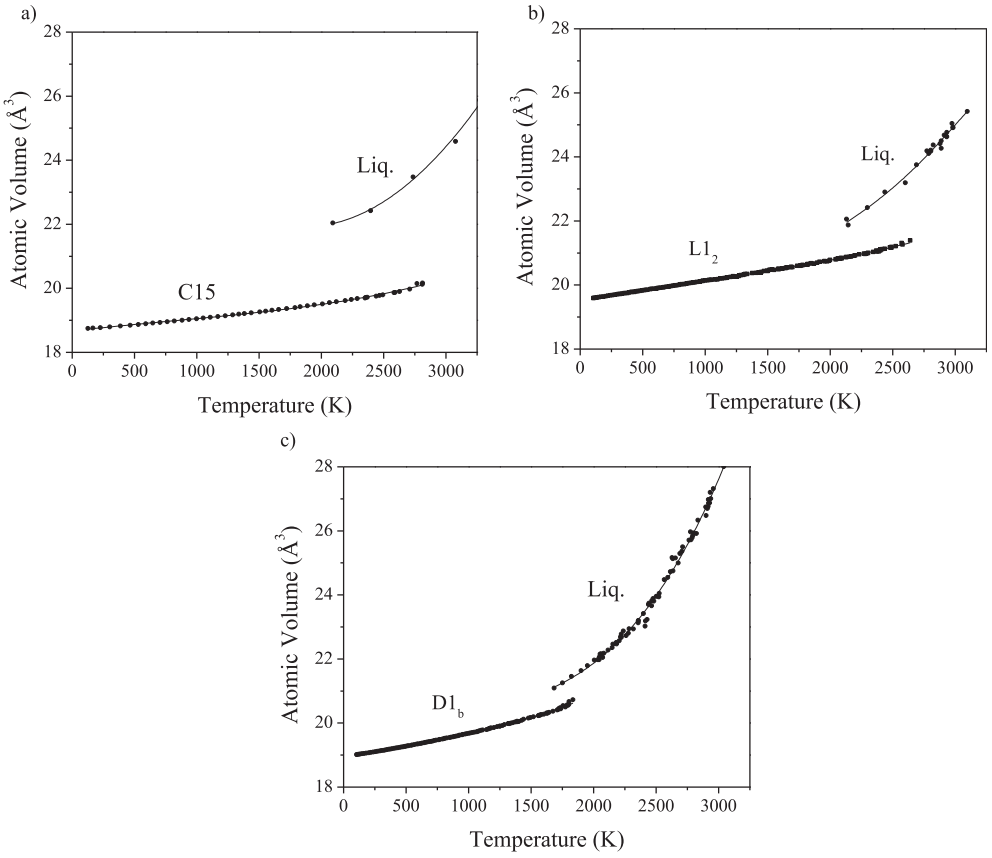

Fig. 4. Atomic volume as a function of temperature for a) Al_2U, b) Al_3U and c) Al_4U.

the thermal stability of the crystal structure for Al_2U and Al_3U is larger than that for Al_4U, which is consistent with experimental evidence [34].

Linear thermal expansion coefficients are calculated by fitting a polynomial to the lattice parameters as a function of *T*. The obtained results are shown in Table 11. Calculated values of the expansion coefficients are a third to a half their corresponding experimentally observed values. It is worth to note that Al_4U shows anomalous temperature behavior along the *b* lattice parameter as in the case of αU [22]. To the authors' knowledge, there is no experimental or theoretical evidence in the literature at this respect. A large disparity between thermal expansions in different directions will certainly produce large stresses in polycrystalline Al_4U and may help to understand why this phase is frequently found in as a gray powder on diffusion experiments [14].

The coexistent phase method has also been applied to study the congruent melting of the Al_2U intermetallic. A long two-phase simulation block of 5184 atoms is built, following a similar procedure as in the case of pure Al (a four cell long block in C15 structure and a four cell long block in liquid state, from the previous Al_2U temperature ramp, joined in the [100] direction). Several constant *NVE* simulations for times between 5×10^3 and 10^4 ps are carried out at slightly different volumes around an initial guess of the melting temperature. New layers of this ordered solid alloy have been observed to grow over the initial solid block under certain conditions (*P* is too high and/or *T* is too low), although the growth velocity is too slow and longer simulation times are needed to reach equilibrium. Therefore, most of the *P* vs *T* equilibrium points come from simulations in which melting of the initial solid occurs. Claussius–Clapeyron equation is used to obtain the following results: $dP/dT = 15.5$ MPa/K, $T_m = 2130$ K, $\Delta\Omega = 1.5$ cm^3/mol, $L = 50$ kJ/mol. The melting temperature is overestimated by around 12.5% of the experimental value [34].

Table 11
Calculated (MEAM) and experimental (Exp.) linear thermal expansions ($\times 10^{-6}$ K^{-1}) for the three intermetallics.

		MEAM	Exp.
Al_2U		5.2	15.1[a]
Al_3U		10.3	15.2[a]
			16.8[b]
			15.9[c]
Al_4U	*a*	35.1	16.5[a]
	b	−18.4	
	c	14.6	
		(10.4 average)	

[a] Ref. [52].
[b] Ref. [53].
[c] Ref. [54].

4.3. Species mobility at infinite dilution

Here, a few selected simulations are presented to test the case of infinite dilution. No systematic studies are carried out, as the only intention is to show the behavior of the fitted potential in such situation. Static CI-NEB (Climbing Image Nudged Elastic Band) calculations and/or constant *NPT* molecular dynamics at the highest possible temperatures have been performed in each phase in order to gain a crude idea of solute mobility.

4.3.1. U diffusion in Al

Blechet et al. [55] measured the diffusion coefficient of U in Al at infinite dilution by fissiography between 798 and 898 K and

observed Arrhenius behavior with activation energy of around 0.29 eV. A few years later, Housseau et al. [56] measured the diffusion coefficient at infinite dilution of U in Al on the order of 10^{-8} cm^2/s between 823 and 903 K. More recent experiments performed by Pérez et al. [57] could not yield any detectable diffusion ($D < 10^{-17}$ cm^2/s) of U into Al at 773 K. The present MEAM potential yields a jump barrier of 1.40 eV for a first neighbor interchange between a U atom and a vacancy in fcc Al, more than twice the value for pure Al, which indicates a very low mobility of U in Al. Consistently, a MD simulation at $T = 900$ K in a block of 500 atoms containing one substitutional U and a vacancy do not show any interchange between these two defects after around 5×10^4 ps.

4.3.2. Al diffusion in U

There are a few experimental works regarding the Al mobility in αU. James and Fern [58] have estimated the diffusion of Al in αU by measuring the growth rate of Al_2U particles from γ quenched adjusted U. They found that the activation energy for diffusion is $Q = 4.0 \pm 2.0$ eV. By using the same technique, Stelly [59] found values close to 1.7 eV, in agreement with values of Smith [60] for high temperatures. In the present work, the energy barriers for the interchange between a neighbor Al atom and the vacancy in αU are calculated for different relative positions (see Ref. [33]). Results are given in Table 12. It can be seen that the lowest energy barriers belong to jumps from 1st and 2nd neighbor positions. They correspond to vacancy movements along the [100] direction and the [001] zigzag direction in αU respectively. Jumps from 3rd and 4th neighbor positions, identified with vacancy jumps with a larger component along [010] direction, yield much higher energy barriers. This behavior is independent of the chemical nature of the jumping atom.

A MD simulation at $T = 900$ K has been made in a block of 720 atoms with one substitutional Al atom close to a vacancy, showing several interchanges after 4×10^4 ps along the compact [100] direction in αU.

Regarding Al mobility in γU, simulations show that the present potential yields a very low diffusivity, independently from the migration mechanism in operation. A simulation at $T = 1400$ K of a small cubic block with 686 atoms containing one substitutional Al atom and a vacancy showed only one interchange with the vacancy after 4.5×10^4 ps. The Al atom in an interstitial position results to be unstable and do not move from its equilibrium substitutional position after a similar simulation time. To the authors' knowledge, there is no available experimental measurement on Al diffusion in γU in the literature.

4.4. Point defects in Al–U intermetallics

4.4.1. Formation energies in Al_4U

There has been a discrepancy in the literature regarding the composition range of existence for Al_4U. Borie [61] found a composition range from 81.8% to 83.1%at Al by chemical analysis but his X-ray measurements suggested a formula Al_4U. He explained the inconsistency by assuming unoccupied U sites. X-ray measurements on Al_4U samples made by Zenou et al. [62] concluded that Al_4U is a typical defect structure with about 10% constitutional vacancies on the U sublattice. Kassner et al. [34] and Wang et al. [63] reflected this result in their reported phase diagrams. Other authors [64] did not find any evidence of constitutional defects and claim that perfect stoichiometry is in effect. This characteristic has been reflected by recent calculations of the Al–U phase diagram [65].

According to the structure of Al_4U [64], there are eight different constitutional point defects in this intermetallic compound (generated from the four Wyckoff positions in the perfect lattice: U atoms at positions 4e and Al atoms at positions 8h, 4e and 4a or Al(1), Al(2) and Al(3) respectively), if only vacancies and antisites are to be considered. The equivalent site for U gives place to one type of U vacancy (V^U) and one Al antisite (Al^U) while the three Al sites originate three different Al vacancies ($V^{Al(1)}$, $V^{Al(2)}$, and $V^{Al(3)}$) and three U antisites ($U^{Al(1)}$, $U^{Al(2)}$, and $U^{Al(3)}$).

To determine their formation energy, each defect has been simulated for block sizes of $3 \times 2 \times 1$ ($N = 120$) and $5 \times 3 \times 2$ ($N = 600$) allowing for full atomic relaxation under periodic boundary conditions. The calculated energy differences with respect to the pure metals are shown in Fig. 5 together with the perfect stoichiometry structure. According to the Wagner–Schottky model [66], the formation enthalpy (per atom) of an off-stoichiometric compound is a linear function of the point defect concentration:

$$\Delta H_f^d = \Delta H_f^{perf} + H_d x_d \tag{9}$$

where ΔH_f^d is the formation enthalpy (per atom) of a cell with N-atoms containing one point defect of type d, ΔH_f^{perf} is the formation enthalpy of a perfect cell, H_d is the formation enthalpy of an isolated point defect of type d and x_d is the atomic concentration of defects. Table 13 reports the values of H_d for each defect in Al_4U obtained by fitting a linear relationship as that given by Eq. (9). Results obtained by first principles calculations by other authors [67] are also shown. Deficiency of Al is dominated by the $U^{Al(2)}$ antisite, while excess of Al by Al^U antisite, in agreement with first principles results [67].

4.4.2. Diffusion in Al–U intermetallics

MD simulations for a system with one vacancy at different temperatures have been performed to calculate the diffusivity by vacancy mechanism in Al_2U, Al_3U and Al_4U. The simulations are made for the same box sizes described in Section 2.4. The temperatures are chosen in the range 800 K $\leq T \leq$ 2000 K, depending on the melting temperature of the given intermetallic. Equilibration

Table 12
Calculated migration energies (in eV) from a n-th vacancy neighbor atom in αU.

Neigh. shell	Al	U [22]
1st	0.47	0.30
2nd	0.71	0.36
3rd	3.25	1.52
4th	2.63	1.25

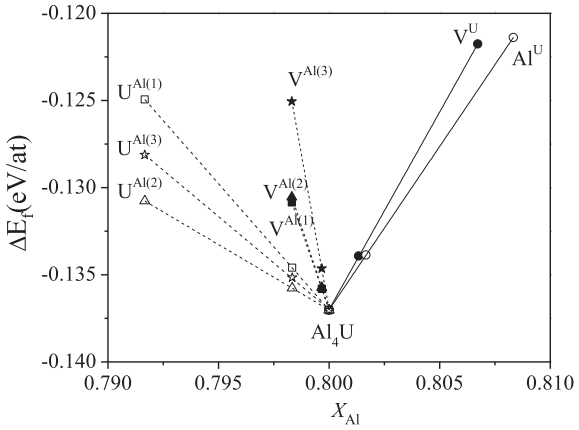

Fig. 5. Vacancy and antisite excess energies for Al_4U. The lower vertex corresponds to perfect Al_4U structure. Symbols farther away from the vertex correspond to small simulation sizes. Lines join systems with the same defect.

Table 13
Calculated (MEAM) and first principles (FP) vacancy and antisite formation energies (eV) for Al_4U.

	Wyckoff position	MEAM		FP [67]	
		Vacancy	Antisite	Vacancy	Antisite
U(1)	4e	2.27	1.87	1.59	1.44
Al(1)	8h	3.67	1.45	1.07	0.27
Al(2)	4e	3.85	0.75	1.93	−0.075
Al(3)	4a	7.12	1.06	1.99	0.62

runs at *NPT* for 5×10^3 ps at each temperature are initially made and their final output configurations subsequently used for longer runs of 5×10^4 ps at *NVE*. During this latter stage, the mobility D^* of each species is calculated similarly as in the case of pure Al. The resulting values are shown in the Arrhenius plots of Fig. 6. Migration energies obtained by fitting the data to an Arrhenius equation are: $E^m = 1.62 \pm 0.06$ for Al_2U, $E^m = 1.05 \pm 0.04$ eV for Al_3U and $E^m_x = 0.90 \pm 0.03$ eV, $E^m_y = 0.91 \pm 0.06$ eV, $E^m_z = 1.09 \pm 0.06$ eV, for Al_4U. The analysis of the MD migration path in each structure to identify individual jump configurations at low temperatures motivated the calculation of migration energies by using the CI-NEB technique. Fig. 7 shows typical vacancy migration paths and statically calculated migration energies for each elementary jump. Vacancy jumps in Al_2U and Al_3U involve first neighbor distances, while for Al_4U several jumps have to be considered. In this latter structure, vacancy migration along the *x* axis is due to a zigzag jump with a static barrier $E^m = 0.65$ eV, while migration along the *y* axis is mainly performed along a compact direction with $E^m = 0.53$ eV, both jumps involving 8h positions. The movement along the *z* axis is accomplished by means of two consecutive jumps along an asymmetric path from 8h to 4a, $E^m = 0.49$ eV, and its reverse, $E^m = 1.18$ eV. The movement along *y* axis between 4a positions is rarely observed even when its static barrier, $E^m = 0.99$ eV, is somewhat lower than the reverse 8h to 4a jump (see Fig. 7c). In Al_2U the static calculation agrees reasonably well with the corresponding MD value. The cases of Al_3U and Al_4U are different in which MD values are higher than those calculated by the static method. It is estimated that entropic contributions, inherent to MD simulations, and a better statistics in obtaining D^* may help to explain the observed differences.

Interface simulations of Al/U (see next section) show that Al diffuses by an interstitial mechanism. In order to characterize this mechanism, MD simulations for a block of Al_3U with an extra Al atom are also made under the same conditions and temperature range as those for the vacancy study. Results are plotted in Fig. 6b, together with vacancy results in the same intermetallic. The corresponding migration energy is $E^m = 0.52 \pm 0.01$ eV. The observed equilibrium configuration is an octahedral site, in which the extra Al atom is positioned at the center of the unit cube and surrounded by six Al neighbors. Its migration mechanism is that of the interstitialcy, in which the interstitial Al pushes one of its neighbors into the next octahedral site, as indicated in Fig. 7b. CI-NEB static calculations yield a value of 0.50 eV which accounts very well for the observed MD activation energy. Interstitials are not usually considered in studies of point defects in intermetallics, although some antecedents exist in the literature. The role of interstitials in diffusion in Ni_2Al_3 compound has been recently stressed by Tingaud and Besson [68]. In particular, Collins and Zacate [69] have included the octahedral interstitial in the calculation of point defect equilibrium concentrations in the $L1_2$ ordered structure.

It is worth to mention that no migration of the U species is observed in any of the performed simulations at the studied temperatures.

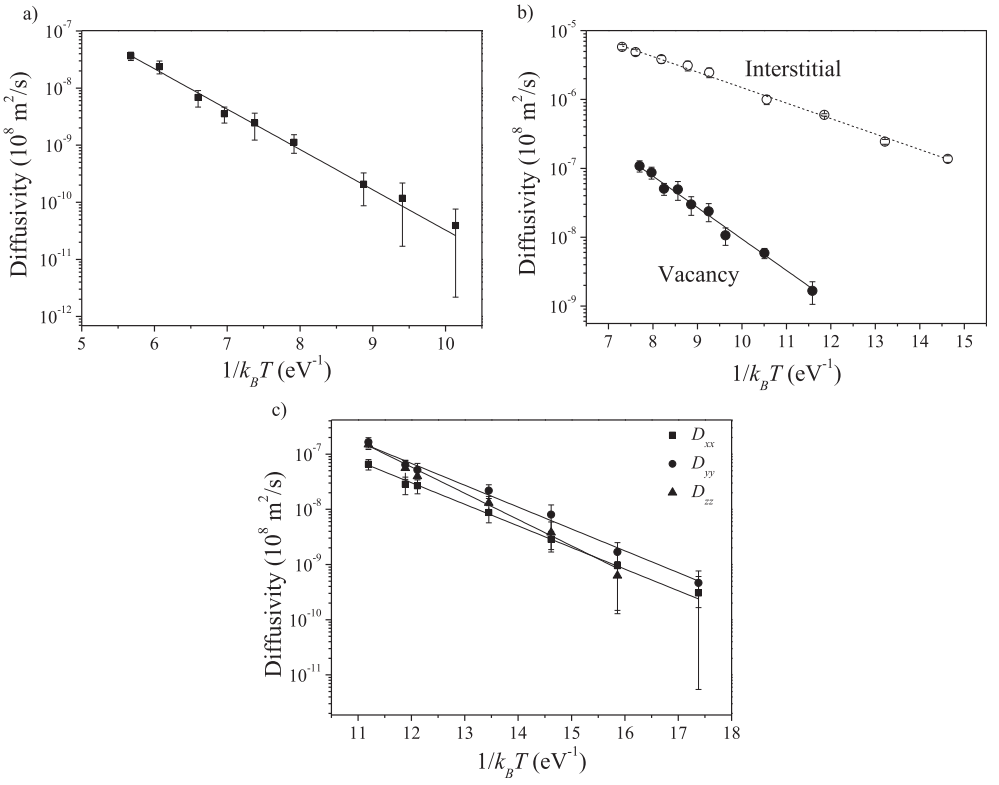

Fig. 6. Al diffusivity in: a) Al_2U, b) Al_3U and c) Al_4U. U diffusivity is not observed.

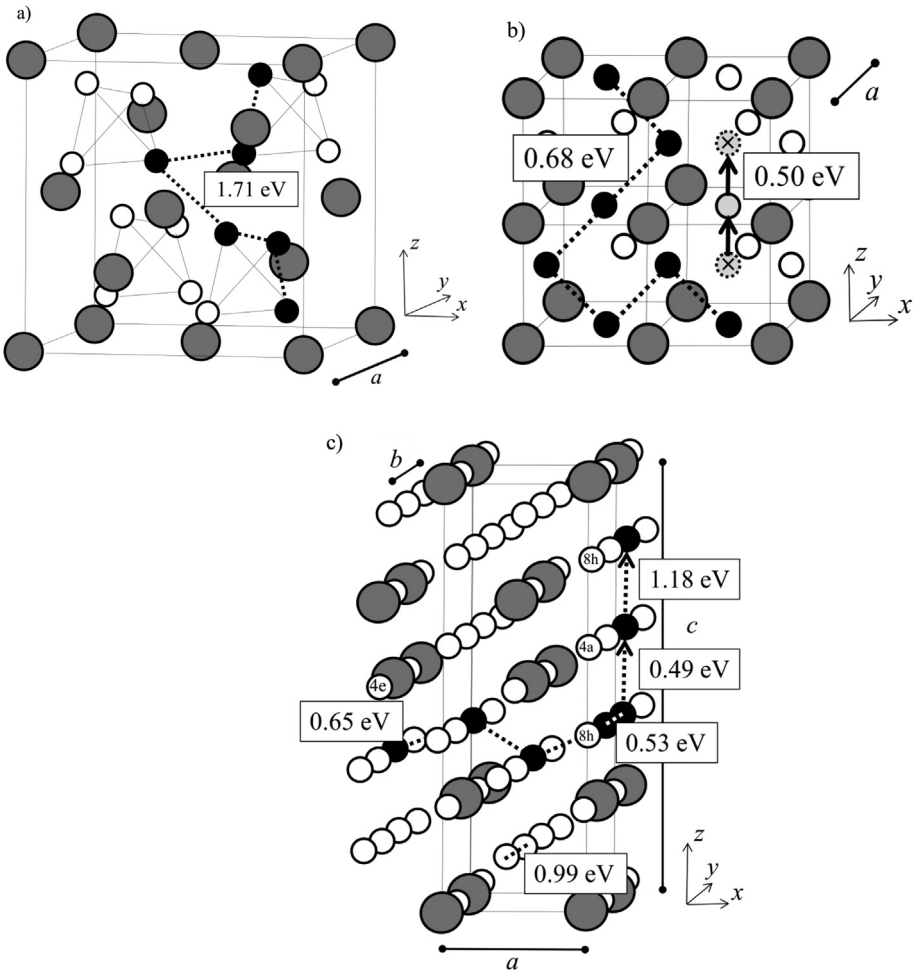

Fig. 7. Observed vacancy jump configurations in a) Al_2U, b) Al_3U and c) Al_4U. Small white (large gray) circles correspond at Al (U) atoms and black circles to moving atoms in a typical migration path. Part b) also includes the interstitial jump studied in Al_3U. The statically calculated migration energies for each elementary jump are also indicated. The dash line stands for a typical migration path. Numbers and letters inside small circles indicate Wyckoff positions in Al_4U.

Interstitial diffusion in Al_2U and Al_4U have not been investigated as they are out of the scope of the present work.

4.5. Al_3U layer growth in a Al/U diffusion couple

The formation of Al_3U in a diffusion couple of Al(Liq.)/γU is studied by MD simulations at the highest possible temperature, avoiding the melting of U. In a first simulation, a large block is constructed by joining two previously equilibrated cells of 3000 Al atoms in liquid state and 1000 U atoms in bcc structure at $T = 1400$ K and $P = 0$, as shown in Fig. 8. The simulation is performed under constant V and rescaling the velocities to keep the temperature constant every around 0.1 ps. No ordered structure is formed after ~10^4 ps at the interface although some U atoms are dissolved into the liquid. By analyzing the atomic displacement between consecutive configurations, it is observed that the atoms in the alloyed layer close to the interface have a low mobility, compared to those at the γU solid. It is in this layer where a new phase is expected to start forming. The low mobility suggests that atoms will take a long time, certainly longer than the extent of simulation, to rearrange themselves spontaneously in an ordered solid, which means a long nucleation time. This behavior depends strongly on the system and it may be taken as a measure of the glass-forming ability of an alloy [70].

To avoid waiting for an apparently long nucleation time, a new system is created in which layers of Al_3U are added to both Al(Liq.)/γU interfaces. Although not directly observed in the previous simulation, it is assumed here that Al_3U is the most probable

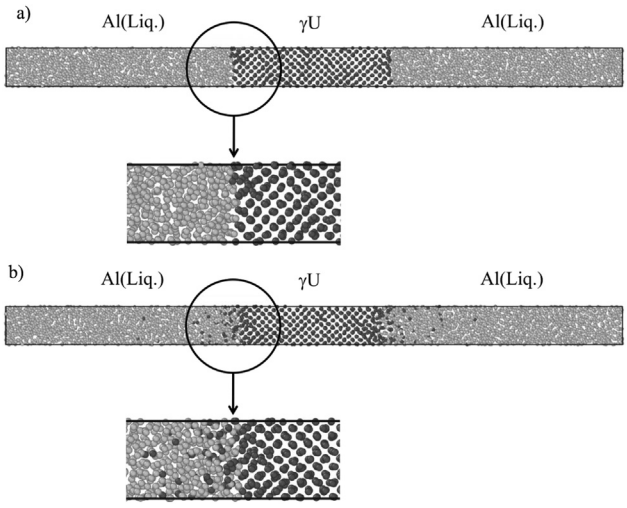

Fig. 8. Simulation of the interface between liquid Al and solid γU at $T = 1400$ K: a) $t = 0$, b) $t = 8 \times 10^3$ ps. Al (U) atoms are represented by light (dark) gray circles.

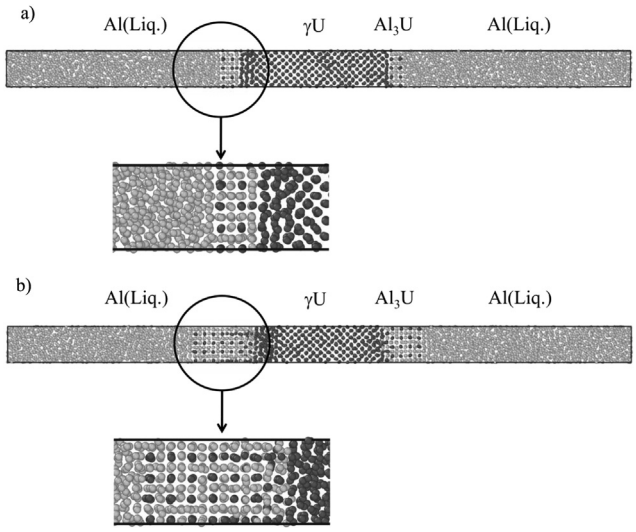

Fig. 9. Simulation of the interface between liquid Al, solid Al_3U and γU at $T = 1400$ K: a) $t = 0$, b) $t = 9 \times 10^4$ ps. Al (U) atoms are represented by light (dark) gray circles.

nucleating phase first, on energetic grounds, as shown by Fig. 1, and second, because it has the smallest unit cell compared to other close competing structures. The *y* and *z* simulation box sizes for γU and Al_3U are chosen so as to have a commensurate interface, i.e., 5 lattice parameters for γU, $a_{\gamma U} = 3.537$ Å, and 4 lattice parameters for Al_3U, $a_{Al3U} = 4.416$ Å, both corresponding to equilibrium values at the simulated temperature and pressure. Previous to a short equilibration of all structures at the same temperature and pressure, it is observed that the intermetallic grows rather fast, by means of Al atoms diffusing through the Al_3U phase. No migration of U atoms has been identified except for a local reordering at the Al_3U/γU interface. The Al migration takes place through an interstitialcy mechanism as already described in the previous section. As atoms are extracted from the pure Al side and deposited into the Al_3U/γU interface region and due to the fact that three Al atoms are needed for each U atom to form an Al_3U unit, the Al_3U phase grows faster towards the Al side rather than into the U side, as can be seen from the snapshot showed in Fig. 9. Such result is in agreement with experimental observation [14,15]. The observed long nucleation time and relatively easier layer growth of Al_3U are also consistent with the experimental evidence [5].

5. Summary and conclusions

In the present work, MEAM interatomic potentials to model pure Al and Al–U alloys have been developed. The potential parameters for Al are fit to literature values of several properties of the ground state fcc structure and a few other metastable states, point defect properties, and the fcc elastic constants. Although other MEAM potentials for pure Al exist in the literature, the one obtained here assures its compatibility with the details of the framework presently adopted, while having a very nice performance with many desired properties. The results obtained for melting properties, stacking faults and point defects diffusivity are consistent with experimental data, the exception being the thermal expansion, which is highly overestimated.

On the other hand, the MEAM potential for the Al–U alloy moderately approximates the lattice parameters and formation energies of Al_2U, Al_3U and Al_4U, but insures a good structure stability of the three intermetallics at realistic temperatures. Elastic properties and thermal expansion are also calculated for the three intermetallics, the obtained results being in modest agreement with available experimental data. Care should be exercised when using these potentials to study mechanical properties. The pronounced anisotropic expansion found for Al_4U is suggested as one possible cause for the lack of bulk integrity of this phase found in experiments.

Although not previously mentioned, the potentials do not produce the correct behavior of the bulk moduli with pressure [48]. Therefore, it is not advisable to use them in simulations under pressures other than those found in normal conditions.

One of the most important applications of the developed interatomic Al–U potential is the study of species diffusivities and diffusion mechanisms in the intermetallics. Simulations of the vacancy diffusivity suggest that Al moves much faster than U in all intermetallics, as usually proposed in the literature. Interestingly, diffusivities in the principal directions on Al_4U do not differ very much in spite of its anisotropic structure.

Finally, the experimental characteristics of the Al_3U growth at the Al/U interface seem to be well represented, although the responsible migration mechanism for Al might deserve further studies.

Acknowledgments

First principles calculations performed by R.C. Pasianot (CNEA/UNSAM/CONICET) are greatfully acknowledged. The authors wish to acknowledge the support of projects PIP 804/10 (CONICET) and C067 (UNSAM).

References

[1] L. Lundberg, J. Nucl. Mater. 167 (1989) 64.
[2] J. Snelgrove, G. Hofman, M. Meyer, C. Trybus, T. Wiencek, Nucl. Eng. Des. 178 (1997) 119.
[3] M.K. Meyer, G.L. Hofman, S.L. Hayes, C.R. Clark, T.C. Wiencek, J.L. Snelgrove, R.V. Strain, K.-H. Kim, J. Nucl. Mater. 304 (2002) 221.
[4] J.M. Hamy, P. Lemoine, F. Huet, B. Guigon, C. Jarousse, J.L. Emin, in: Proceedings of the 8th International Topical Meeting on Research Reactor Fuel Management (RRFM), Munich, 2004.
[5] D. Subramanyam, M.R. Notis, J.I. Godstein, Metall. Trans. A 16 (1985) 589.
[6] M.I. Mirandou, S.N. Balart, M. Ortiz, M.S. Granovsky, J. Nucl. Mater. 323 (2003) 29.
[7] F. Mazaudier, C. Proye, F. Hodaj, J. Nucl. Mater. 377 (2008) 476.
[8] M.I. Mirandou, S. Aricó, M. Rosenbusch, M. Ortiz, S. Balart, L. Gribaudo, J. Nucl. Mater. 384 (2009) 268.
[9] Yeon Soo Kim, G.L. Hofman, H.L. Ryu, J. Rest, in: Proceedings of the 27th International Meeting of Reviews Reduced Enrichment for Research and Test Reactors (RERTR), Boston, 2005.
[10] J.M. Park, H.J. Ryu, S.J. Oh, D.B. Lee, C.K. Kim, Y.S. Kim, G.L. Hofman, J. Nucl. Mater. 374 (2008) 422.
[11] D.W. Bareis, US Atomic Energy Commission Publication, AECD-3795, 1949.
[12] J.R. Murray, Tech. Rep., AERE-M/R-799, UK, 1951.
[13] S. Storchheim, J. Zambrow, Tech. Rep. SEP-102, USA, 1952.
[14] A.D. Le Claire, I.J. Bear, J. Nucl. Energy 2 (1956) 229.
[15] L.S. Deluca, H. T. Sumsion, Tech. Rep., KAPL-1747, USA, 1957.
[16] L.S. Castleman, J. Nucl. Mater. 3 (1961) 1.
[17] M.I. Baskes, Phys. Rev. B 46 (1992) 2727.
[18] B.-J. Lee, M.I. Baskes, Phys. Rev. B 62 (2000) 8564;
B.-J. Lee, M.I. Baskes, H. Kim, Y.K. Cho, Phys. Rev. B 64 (2001) 184102.
[19] B.-J. Lee, J.-H. Shim, M.I. Baskes, Phys. Rev. B 68 (2003) 144112.
[20] B. Jelinek, J. Houze, S. Kim, M.F. Horstemeyer, M.I. Baskes, S.-G. Kim, Phys. Rev. B 75 (2007) 054106.
[21] B. Jelinek, S. Groh, M.F. Horstemeyer, J. Houze, S.-G. Kim, G.J. Wagner, A. Moitra, M.I. Baskes, Phys. Rev. B 85 (2012) 245102.
[22] J.R. Fernández, M.I. Pascuet, Model. Simul. Mater. Sci. Eng. 22 (2014) 055019.
[23] S.J. Plimpton, J. Comp. Phys. 117 (1995) 1. http://lammps.sandia.gov.
[24] P.M. Gullett, G.J. Wagner, A. Slepoy, M.F. Horstemeyer, H. Fang, M. Li, M.I. Baskes, SANDIA Report, 2003, p. 8782.
[25] J.H. Rose, J.R. Smith, F. Guinea, J. Ferrante, Phys. Rev. B 29 (1984) 2963.
[26] S.A. Teukolsky, W.T. Vetterling, B.P. Flannery (Eds.), Numerical Recipes in Fortran 77: The Art of Scientific Computing, W.H. Press, Cambridge Univ. Press, New York, 1997.
[27] C. Kittel, Introduction to Solid State Physics, Wiley Interscience, New York, 1986.
[28] J.C. Boettger, S.B. Trickey, Phys. Rev. B 53 (1996) 3012.

[29] R.C. Pasianot, SIESTA Calculations, Personal communication.
[30] Y. Mishin, D. Farkas, M.J. Mehl, D.A. Papaconstantopoulos, Phys. Rev. B 59 (1999) 3393.
[31] Landolt-Börnstein, in: H. Ullmaier (Ed.), Numerical Data and Functional Relationships in Science and Technology, New Series, vol. III/25, Springer-Verlag, Berlin, 1991.
[32] G.N. Kamm, G.A. Alers, J. Appl. Phys. 35 (1964) 327.
[33] M.I. Pascuet, G. Bonny, J.R. Fernández, J. Nucl. Mater. 424 (2012) 158.
[34] M.E. Kassner, P.H. Adler, M.G. Adamson, D.E. Peterson, J. Nucl. Mater. 167 (1989) 160.
[35] Shu-ying Kang, Tao Gao, Xiao-feng Tian, Physica B 407 (2012) 748.
[36] P.R. Alonso, J.R. Fernández, P.H. Gargano, G.H. Rubiolo, Physica B 404 (2009) 2851.
[37] L. Kniznik, P.R. Alonso, P.H. Gargano, M.D. Forti, G.H. Rubiolo, Proc. Mater. Sci. 1 (2012) 514.
[38] Z. Nourbakhsh, J. Supercond. Nov. Magn. 24 (2011) 879–886.
[39] A.B. Belonoshko, N.V. Skorodumova, A. Rosengren, B. Johansson, Phys. Rev. B 73 (2006) 012201.
[40] N.W. Ashcroft, N.D. Mermin, Solid State Physics, Holt, Rinehart & Winston, New York, 1976.
[41] P.M. Nash, S.G. Steinemann, Phys. Chem. Liq. 29 (1995) 43 and references therein.
[42] J.R. Morris, C.Z. Wang, K.M. Ho, C.T. Chan, Phys. Rev. B 49 (1994) 3109.
[43] A. Hänström, P. Lazor, J. Alloy Compd. 305 (2000) 204.
[44] P.D. Desai, Int. J. Thermophys. 8 (1987) 621.
[45] C.M. Saeger Jr., E.J. Ash, Bureau Stand. J. Res. 8 (1932) 37.
[46] J.L. Tallon, A. Wolfenden, J. Phys. Chem. Solids 40 (1979) 831.
[47] B. Hammer, K.W. Jacobsen, V. Milman, M.C. Payne, J. Phys. Condens. Matter 4 (1992) 10453.
[48] N.V. Chandra Shekar, P.Ch. Sahu, M. Rajagopalan, M. Yousuf, K. Govinda Rajan, J. Phys. Condens. Matter 9 (1997) 5867.
[49] L. Kniznik, P.R. Alonso, P.H. Gargano, G.H. Rubiolo, in: Proceedings of the 33th International Meeting of Reviews Reduced Enrichment for Research and Test Reactors (RERTR), Santiago of Chile, 2011.
[50] J.P. Itié, J.S. Olsen, L. Gerward, U. Benedict, J.C. Spirlet, Physica B 139–140 (1986) 330.
[51] P.C. Sahu, V. Chandra Shekar, Pramana 54 (2000) 685.
[52] T.R.G. Kutty, C. Ganguly, D.H. Sastry, J. Nucl. Mater. 226 (1995) 197.
[53] R.J. Pearce, J. Nucl. Mater. 17 (1965) 201.
[54] Y.S. Touloukian, R.K. Kirby, R.E. Taylor, P.D. Desai, Thermal Expansion: Metallic Elements and Alloys, Plenum, New York, 1975.
[55] J.J. Blechet, A. Van Craeynest, D. Calais, J. Nucl. Mater. 27 (1968) 112.
[56] N. Housseau, A. Van Craeynest, D. Calais, J. Nucl. Mater. 39 (1971) 189.
[57] R.A. Perez, J. Gordillo, N. Di Lalla, Measurement 45 (2012) 1836.
[58] P.F. James, F.H. Fern, J. Nucl. Mater. 29 (1969) 203.
[59] M. Stelly, J. Nucl. Mater. 40 (1971) 84.
[60] A.F. Smith, J. Nucl. Mater. 27 (1968) 194.
[61] B.S. Borie, Trans. AIME 191 (1951) 800.
[62] V.Y. Zenou, G. Kimmel, C. Cotler, M. Aizenshtein, J. Alloys Compd. 329 (2001) 189.
[63] J. Wang, X. Liu, C. Wang, J. Nucl. Mater. 374 (2008) 79.
[64] O. Tougait, H. Noël, Intermetallics 12 (2004) 219.
[65] D. Sedmidubský, R.J.M. Konings, P. Souček, J. Nucl. Mater. 397 (2010) 1.
[66] C. Wagner, Thermodynamics of Alloys, Addison-Wesley, Cambridge, MA, 1952.
[67] L. Kniznik, P.R. Alonso, P.H. Gargano, G.H. Rubiolo, Unpublished results.
[68] D. Tingaud, R. Besson, Intermetallics 45 (2014) 38.
[69] G.S. Collins, M.O. Zacate, Hyperf. Interact. 136 (137) (2002) 641.
[70] Chunguang Tang, P. Harrowell, Nat. Mater. Lett. 12 (2013) 507.